^{68}Ga-DOTANOC PET/CT for Baseline Evaluation of Patients with Head and Neck Paraganglioma

Punit Sharma[1], Alok Thakar[2], Sudhir Suman KC[1], Varun Singh Dhull[1], Harmandeep Singh[1], Niraj Naswa[1], Rama Mohan Reddy[1], Sellam Karunanithi[1], Rajeev Kumar[1], Rakesh Kumar[1], Arun Malhotra[1], and Chandrasekhar Bal[1]

[1]Department of Nuclear Medicine, All India Institute of Medical Sciences, New Delhi, India; and [2]Department of Otorhinolaryngology, All India Institute of Medical Sciences, New Delhi, India

The purpose of this study was to evaluate the role of ^{68}Ga-labeled DOTANOC PET/CT for baseline evaluation of patients with head and neck paragangliomas (HNPs). **Methods:** The data for 26 patients (mean age ± SD, 34.3 ± 10.4 y; 50% men) with known or suspected HNPs who underwent ^{68}Ga-DOTANOC PET/CT for staging were retrospectively analyzed. PET/CT was performed after intravenous injection of 132–222 MBq of ^{68}Ga-DOTANOC. The images were evaluated by 2 experienced nuclear medicine physicians in consensus, both qualitatively and quantitatively. The PET/CT findings were grouped as HNPs, paraganglioma at other sites (non-HNPs), and metastatic disease. The size and maximum standardized uptake values (SUVmax) were measured for all lesions. All of the patients also underwent whole-body ^{131}I-metaiodobenzylgunanidine (^{131}I-MIBG) scintigraphy and conventional imaging (CT/MR imaging) of the head and neck region. Their results were compared with those of ^{68}Ga-DOTANOC PET/CT. **Results:** ^{68}Ga-DOTANOC PET/CT findings were positive in all 26 patients, and 78 lesions were detected. PET/CT imaging demonstrated 45 HNPS, 10 non-HNPs, and 23 metastatic sites. Fifteen patients (57.6%) had more than one site of disease on PET/CT. Among 45 HNPs, 26 were carotid body tumors (CBTs), 15 glomus jugulare, 3 glomus tympanicum, and 1 laryngeal paraganglioma. A positive correlation was seen between size and SUVmax of HNPs ($\rho = 0.323$; $P = 0.030$). The SUVmax of the CBTs was higher than that of jugulotympanic paragangliomas ($P = 0.026$). No correlation was seen between size and SUVmax ($\rho = 0.069$; $P = 0.854$) of non-HNPs. The size and SUVmax of non-HNPs were significantly less than those of HNPs ($P = 0.029$ and 0.047, respectively). ^{131}I-MIBG scintigraphy showed only 30 of the 78 lesions and was inferior to PET/CT ($P < 0.0001$). Conventional imaging (CT/MR imaging) was positive for 42 of 49 head and neck lesions and was inferior to PET/CT on direct comparison ($P = 0.015$). A combination of CT/MR imaging and ^{131}I-MIBG scintigraphy detected only 53 of 78 (67.9%) lesions and was also inferior to PET/CT ($P < 0.0001$). **Conclusion:** ^{68}Ga-DOTANOC PET/CT is useful for the baseline evaluation of patients with HNPs and can demonstrate synchronous paragangliomas at other sites and distant metastases. It is superior to ^{131}I-MIBG scintigraphy and conventional imaging (CT/MR imaging) for this purpose.

Received Oct. 10, 2012; revision accepted Dec. 4, 2012.

For correspondence or reprints contact: Chandrasekhar Bal, Department of Nuclear Medicine, All India Institute of Medical Sciences, Ansari Nagar, New Delhi-110029, India

E-mail: csbal@hotmail.com

Published online Mar. 21, 2013.

Key Words: head and neck paraganglioma; ^{68}Ga-DOTANOC; PET/CT; staging; ^{131}I-MIBG

J Nucl Med 2013; 54:841–847
DOI: 10.2967/jnumed.112.115485

Head and neck paragangliomas (HNPs) are rare hypervascular tumors, representing less than 0.5% of all head and neck neoplasms (*1*). Approximately 3% of paragangliomas occur in the head and neck area (*2*). HNPs are derived from the parasympathetic nervous system and can be present in a variety of locations, including the carotid body (carotid body tumors [CBTs] or glomus caroticum), vagus nerve (glomus vagale), jugular bulb (glomus jugulare), and tympanic branch of the ascending pharyngeal artery (glomus tympanicum) (*3*). HNPs can also arise at other locations, such as the ciliary glomus or laryngic glomus. HNPs are usually benign and grow slowly, causing symptoms by compressing adjacent structures. In contrast to paragangliomas at other sites, only 1%–3% of HNPs secrete catecholamines (*4*). More importantly, approximately 6%–19% of HNPs are malignant, as evidenced by the presence of regional or distant metastases (*3*). About 90% of HNPs are sporadic, whereas the remaining are familial (*5*). The latter are important because they are often multicentric and associated with paragangliomas at other sites.

Imaging can be considered in patients who present with clinical symptoms suggestive of HNPs or in individuals from families with hereditary paragangliomas. It is necessary not only to detect and characterize the lesion but also to study the presence of multiplicity (*6*). MR imaging with MR angiography is considered the investigation of choice, because of the better soft-tissue contrast of this modality than CT imaging (*6*). However, CT is superior to MR imaging for demonstrating associated bone destruction. Unfortunately, the specificity of both MR imaging and CT remains low, with a long list of differential diagnoses (schwannomas, lymph nodes, salivary gland tumors, aneurysm, hypervascular metastasis, giant cell tumors, or osteodural arteriovenous malformation) (*7*). The gold standard for the detection of HNPs, especially small lesions, although

invasive, is still digital subtraction angiography (*8*). In addition, whole-body screening for metastasis or other paragangliomas is not practical with CT/MR imaging and has low sensitivity. These limitations of anatomic modalities highlight the need for a specific functional whole-body imaging technique.

Radioisotope imaging with ^{123}I-/^{131}I-metaiodobenzylguanidine (^{123}I-/^{131}I-MIBG) or ^{111}In-diethylenetriamine-pentaacetic acid (DTPA)-pentetreotide with SPECT or SPECT/CT is useful for whole-body screening in the case of metastatic or familial paragangliomas (*9*). The sensitivity of ^{123}I-/^{131}I-MIBG imaging is lower in extraadrenal paragangliomas, metastatic paragangliomas, and recurrences. Because HNPs are usually noncatecholamine-producing, ^{123}I-/^{131}I-MIBG scintigraphy has a low sensitivity for such tumors (*10*). Somatostatin receptor scintigraphy (SRS) with ^{111}In-DTPA-pentetreotide scintigraphy is superior to ^{123}I-/^{131}I-MIBG for HNPs but suffers from the drawbacks of limited resolution and low sensitivity of SPECT imaging (*11,12*). ^{68}Ga-labeled DOTANOC is a PET tracer for somatostatin receptor (SSTR) imaging, providing the advantages of better resolution, higher sensitivity, and quantification ability of PET technology (*13*). In a few studies with a small number of patients with HNPs, ^{68}Ga-DOTANOC PET/CT has shown promising results (*13–15*). However, there is no systematic study evaluating ^{68}Ga-DOTANOC PET/CT in HNPs. Therefore, the objective of the present study was to evaluate the usefulness of ^{68}Ga-DOTANOC PET/CT for the baseline evaluation of HNPs. In addition, we also compared ^{68}Ga-DOTANOC PET/CT with ^{131}I-MIBG (^{123}I-MIBG is not available in our country) scintigraphy and conventional imaging (CT/MR imaging), when available.

MATERIALS AND METHODS

This was a retrospective study. Approval from the institutional ethical committee was obtained. Because of retrospective nature of the study, written informed consent was waived. The data from patients with known or suspected HNPs who underwent staging with ^{68}Ga-DOTANOC PET/CT between July 2007 and July 2012 were retrospectively evaluated. The inclusion criteria were known (biopsy) or suspected (imaging) HNP and no primary treatment. Exclusion criteria were any form of primary treatment, other neuroendocrine tumors of head and neck, or lack of definite reference standard. Twenty-six patients met these criteria. The data for these 26 patients were retrieved from a department registry and analyzed.

^{68}Ga-DOTANOC Synthesis

^{68}Ga-DOTANOC was synthesized as previously described by Zhernosekov et al. (*16*) and is briefly summarized here. ^{68}Ge/^{68}Ga (1,110–1,850 MBq [30–50 mCi]) was eluted from a generator (Cyclotron Co Ltd.) using 0.1 M HCl. The eluent was loaded on a miniaturized column of organic cation-exchanger resin to preconcentrate and prepurify (using 80% acetone/0.15 M HCl). The processed ^{68}Ga (half-life, 68.3 min; positron branching fraction, 88%; effective positron energy maximum, 1.9 MeV) was directly eluted with 97.7% acetone/0.05 M HCl into the reaction vial containing 30–50 μg of DOTANOC. Synthesis was performed at approximately 126°C for 10–15 min, followed by removal of labeled peptide from unlabeled peptide using a reversed-phase C-18 column with 400 μL of ethanol. This solution was further diluted with normal saline and passed through a 0.22-μm filter to obtain a sterile preparation for injection. A labeling yield of more than 95% was achieved after 10–15 min of heating.

^{68}Ga-DOTANOC PET/CT Acquisition

^{68}Ga-DOTANOC PET/CT was performed on a dedicated scanner (Biograph 2; Siemens Medical Solutions). Fasting was not mandatory. A dose of 132–222 MBq (4–6 mCi) of ^{68}Ga-DOTANOC was injected intravenously. After a 45- to 60-min uptake period, the patients were taken for PET/CT acquisition. On the PET/CT system, CT images were acquired on a spiral dual-slice CT device (slice thickness of 4 mm, pitch of 1, matrix of 512 × 512 pixels, and pixel size of 1 mm). After CT acquisition, the table was moved toward the field of view of PET, and PET acquisition of the same axial range was started with the patient in the same position. The PET components of the PET/CT are based on a full-ring lutetium oxyorthosilicate PET system. Three-dimensional PET images were acquired from the base of skull (including pituitary fossa) to mid thighs. Additional spot views were taken when necessary. PET data were acquired using a matrix of 128 × 128 pixels with a slice thickness of 1.5 mm. CT-based attenuation correction of the emission images was used. PET images were reconstructed by an iterative method, ordered-subset expectation maximization (2 iterations and 8 subsets). After completion of the PET acquisition, the reconstructed attenuation-corrected PET images, CT images, and fused images of matching pairs of PET and CT images were available for review in the axial, coronal, and sagittal planes and in maximum-intensity projections, 3-dimensional cine mode.

Image Analysis

^{68}Ga-DOTANOC PET/CT studies were evaluated by 2 experienced nuclear medicine physicians in consensus. They were aware of the primary diagnosis (HNP) but not the site and were masked to the findings of structural imaging. PET/CT images were evaluated both qualitatively and semiquantitatively, and images were assessed for nonphysiologic focal areas of increased ^{68}Ga-DOTANOC uptake. Any such uptake higher than mediastinal blood pool was taken as positive. Positive findings on ^{68}Ga-DOTANOC PET were localized to anatomic images from the CT scan. The PET/CT findings were grouped as HNPs, paraganglioma at other sites (non-HNPs), and metastatic disease. The size and maximum standardized uptake values (SUVmax) were measured for all lesions. The standardized uptake value was calculated via the default method by body weight: [(standardized uptake value = mean region of interest activity [MBq/g]/injected dose [MBq])/body weight [g]].

^{131}I-MIBG Imaging

All of the patients also underwent ^{131}I-MIBG scintigraphy with or without SPECT/CT within ±2 wk of PET/CT. None of the patients had received any drugs that would interfere with ^{131}I-MIBG uptake, such as tricyclic antidepressants, or sympathomimetic amines. After the intravenous injection of a mean dose (37 ± 12 MBq) of ^{131}I-MIBG (GE Healthcare), planar scintigraphic images were obtained with a large-field-of-view dual-head γ-camera (Symbia E; Siemens Medical Solutions) and a high-energy collimator. Whole-body images in the ventral and dorsal planes and target images of the head and neck were acquired at 48 h after injection. In 11 patients, SPECT of the head and neck was performed with the following parameters: 128 × 128 matrix, 120 projections

in 3° angle increments, and an acquisition time of 40 s per projection. The SPECT scanning was followed by CT examination, with the following acquisition parameters: 130 kV, 100 mAs, a pitch of 1, and a 512 × 512 matrix using standard filters. All SPECT/CT images were uniformly processed with commercially available E.soft (Siemens Medical Solutions) software on a Syngo nuclear medicine workstation (Siemens Medical Solutions). ^{131}I-MIBG images were evaluated by 2 experienced nuclear medicine physicians in consensus. The physicians were aware of the primary diagnosis (HNP) but masked to the site and results of conventional imaging.

Conventional Imaging

Conventional imaging for HNPs at our center includes anatomic imaging of the head and neck with contrast-enhanced CT with CT angiography or contrast-enhanced MR imaging with MR angiography. The results of CT/MR imaging were collected from a department registry. CT was performed in 22 patients and MR imaging in 6 patients. These images were not revaluated, and final reports were used for analysis.

Reference Standard

Because of the high risk of complications associated with biopsy and contraindication to surgery in many, histopathology was not available for all lesions, though this would have been ideal. Also, it was not ethically feasible. For HNP, biopsy (n = 22), digital subtraction angiography (n = 3), or characteristic appearance on conventional imaging (n = 22) was taken as the reference standard. For non-HNPs, biopsy (n = 1) and the combination of imaging and urinary or serum catecholamines (n = 9) were taken as the reference standard. For metastatic lesions, a combination of histopathology (n = 4) and imaging follow-up (n = 19) was used as reference standard. The minimum duration of imaging follow-up was 6 mo from PET/CT.

Statistical Analysis

Statistical analysis was done using SPSS (version 11.5; SPSS Inc.). Categoric variables were expressed using number and percentage. Descriptive statistics such as mean, median, and SD were used for continuous variables. The Kolmogorov–Smirnov test was used to check the normality of the data. The Mann–Whitney test with 2-tailed probability was used to compare continuous variables among groups. The Spearman rank correlation coefficient was used to look for any relation between tumor size and SUVmax. The McNemar test was used to compare the diagnostic performance of ^{68}Ga-DOTANOC PET/CT with ^{131}I-MIBG and conventional imaging. A P value of less than 0.05 was taken as significant.

RESULTS

Patient Characteristics

Twenty-six patients were included for final analysis (mean age ± SD, 34.3 ± 10.4 y; median age, 34.5 y; age range, 16–59 y). Fifty percent of the patients were men. A painless neck mass was the most common presentation (n = 25). One patient presented with pulsatile tinnitus. Only 2 patients were hypertensive. Overall, 4 patients had elevated serum or urinary catecholamine levels, including 3 who also had additional non-HNPs. Of the total 26 patients, 14 patients underwent surgery for the HNPs.

^{68}Ga-DOTANOC PET/CT Results

Overall. ^{68}Ga-DOTANOC PET/CT findings were positive in all 26 patients, and 78 lesions were detected. Fifteen patients (57.6%) had more than one site of disease on PET/CT. ^{68}Ga-DOTANOC PET/CT demonstrated 45 HNPS, 10 non-HNPs, and 23 metastatic sites. The overall mean SUVmax of the lesions was 39.9 ± 51.3 (median, 15.5; range, 1.1–200.3). The overall mean size of the lesions was 3.4 ± 2.4 cm (median, 2.6 cm; range: 0.5–10.7 cm). No overall correlation was seen between lesion size and SUVmax (ρ = 0.027; P = 0.936).

HNP. ^{68}Ga-DOTANOC PET/CT demonstrated 45 HNPs: 26 (57.7%) were CBTs, 15 (33.3%) were glomus jugulare, 3 (6.6%) were glomus tympanicum, and 1 (2.8%) was laryngeal paraganglioma. Eight (30.7%) CBTs, 11 (73.3%) glomus jugulare, all glomus tympanicum, and the laryngeal paraganglioma were unilateral. The remaining CBTs (18/26) and glomus jugulare (4/15) were bilateral. The size and SUVmax of the lesions are detailed in Table 1. A significant positive correlation was seen between size and SUVmax of HNPs (ρ = 0.323; P = 0.030). The SUVmax of the CBTs was significantly higher than that of jugulotympanic paragangliomas (P = 0.026). However, no such difference was seen for size (P = 0.129). Bone erosion on the CT part of

TABLE 1
Size and SUVmax of Various Groups of Lesions Seen on ^{68}Ga-DOTANOC PET/CT

Lesion	SUVmax			Size (cm)		
	Mean ± SD	Median	Range	Mean ± SD	Median	Range
HNP	42.2 ± 53.8	15.5	1.2–189.9	4.06 ± 2.3	3.7	0.8–10.7
CBT	51.6 ± 60.5	26.1	2.5–189.9	4.3 ± 1.9	4.6	1–8.5
Jugulotympanic paraganglioma*	22.6 ± 29.7	7.6	1.2–95.2	3.6 ± 2.9	2.6	0.8–10.7
Laryngeal paraganglioma†	150			2.6		
Non-HNP	14.4 ± 23.1	5.63	1.1–75.9	2.3 ± 1.1	1.9	1.2–4.2
Metastasis	49.4 ± 54.1	23.9	5.9–200.3	2.2 ± 2.2	1.4	0.5–8.7

*15 glomus jugulare and 3 glomus tympanicum.
†Solitary lesion.

the PET/CT examination was seen, which was associated with 18 HNPs including minimal erosion with 7.

Non-HNPs. ^{68}Ga-DOTANOC PET/CT also detected 10 non-HNPs in 3 of 26 patients. Of these 10, 5 were retroperitoneal paragangliomas (50%), 2 were adrenal paragangliomas (i.e., pheochromocytoma [20%]), 2 were aortic body tumors (20%), and 1 was posterior mediastinal paraganglioma (10%). The size and SUVmax of the non-HNPs are detailed in Table 1. No significant correlation was seen between size and SUVmax ($\rho = 0.069$; $P = 0.854$). Both size and SUVmax of non-HNPs were significantly less than those of HNPs ($P = 0.029$ and 0.047, respectively) (Fig. 1).

Metastases. ^{68}Ga-DOTANOC PET/CT demonstrated 23 metastatic sites in 6 of 26 patients. Only 1 of these 6 patients also had a non-HNP (retroperitoneal paraganglioma). The most common site of metastasis was bone (10/23; 43.4%), followed by liver (9/23; 39.1%), lymph node (3/23; 13%), and tumor thrombus in the jugular vein (1/23; 4.5%). The size and SUVmax of metastatic lesions are detailed in Table 1. No correlation was seen between size and SUVmax of metastatic lesions ($\rho = 0.152$; $P = 0.575$). The size of metastatic lesions was less than that of paragangliomas ($P = 0.001$), but the SUVmax was significantly higher ($P = 0.050$) (Fig. 1).

Comparison with ^{131}I-MIBG Scintigraphy

^{131}I-MIBG scintigraphy findings were positive for only 30 (38.4%) of the 78 lesions detected by ^{68}Ga-DOTANOC PET/CT. It failed to demonstrate the remaining 48 (61.6%) lesions. Overall, ^{131}I-MIBG scintigraphy was inferior to PET/CT ($P < 0.0001$) (Figs. 2–4). Also, no additional lesions were demonstrated by ^{131}I-MIBG scintigraphy; findings were positive for only 16 of 45 (35.5%) HNPs, 6 of 10 (60%) non-HNPs, and 4 of 23 (17.3%) metastatic sites. ^{131}I-MIBG scintigraphy was inferior to ^{68}Ga-DOTANOC PET/CT for HNPs ($P < 0.0001$) and metastases ($P < 0.0001$) but not for non-HNPS ($P = 0.125$) (Fig. 3). Among HNPs, ^{131}I-MIBG scintigraphy results were positive for only 14 of 26 (53.8%) CBTs, 1 of 15 (6.6%) glomus jugulare, 1 of 1 laryngeal paraganglioma, and none of the 3 glomus tympanicum. It was inferior to ^{68}Ga-DOTANOC PET/CT for both CBTs ($P = 0.0005$) and jugulotympanic paragangliomas ($P < 0.0001$).

Comparison with CT/MR Imaging

Comparable anatomic head and neck imaging (CT/MR imaging) done within ±2 wk was available for 49 lesions seen on ^{68}Ga-DOTANOC PET/CT (45 HNPs, 3 nodal metastases, and 1 tumor thrombus). Conventional imaging was positive for 42 (85.7%) of these 49 lesions. CT (available for 42 lesions) was negative for 7 lesions, including 2 CBTs, 2 glomus jugulare, 2 glomus tympanicum, and 1 tumor thrombosis. When available, MR imaging demonstrated all the head and neck lesions seen on ^{68}Ga-DOTANOC PET/CT ($n = 7$). On direct lesion-wise comparison, ^{68}Ga-DOTANOC PET/CT was superior to conventional imaging ($P = 0.015$). A combination of conventional imaging and ^{131}I-MIBG scintigraphy detected only 53 of 78 (67.9%) lesions seen on PET/CT and no additional lesions. This combination was inferior to ^{68}Ga-DOTANOC PET/CT ($P < 0.0001$).

DISCUSSION

The baseline evaluation of HNPs is usually performed with CT or MR imaging to define the location and extent and to detect synchronous HNPs (*9*). Functional imaging is probably not necessary in the preoperative work-up of patients with negative genetic testing (*9*). However, because the genetic status is often not available before surgery, the possibility of multifocal or metastatic disease should be considered (or excluded) in all cases, and radioisotope imaging

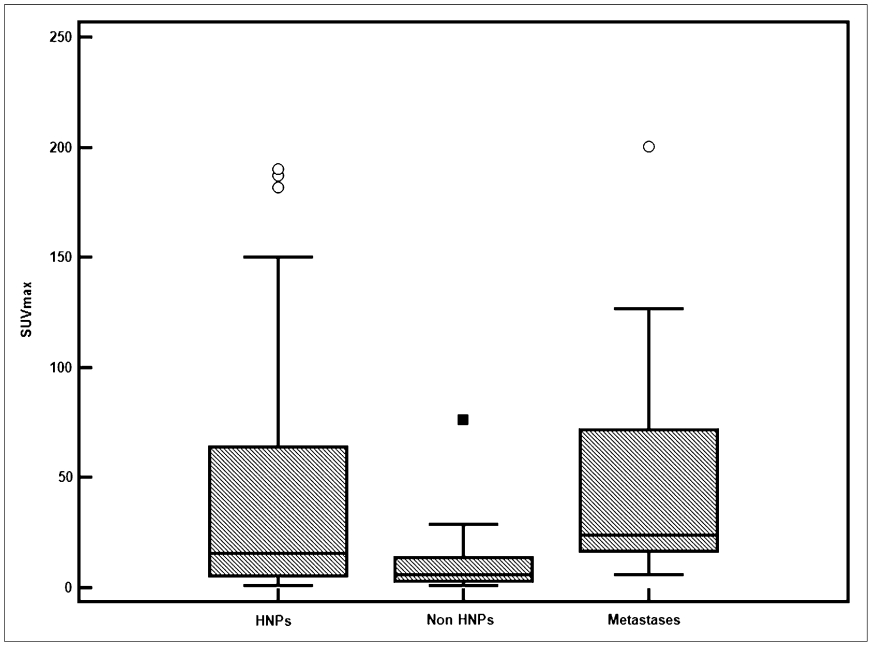

FIGURE 1. Box-and-whiskers plots comparing SUVmax of HNPs, non-HNPs, and metastases. ○ = outliers; ■ = extreme outlier.

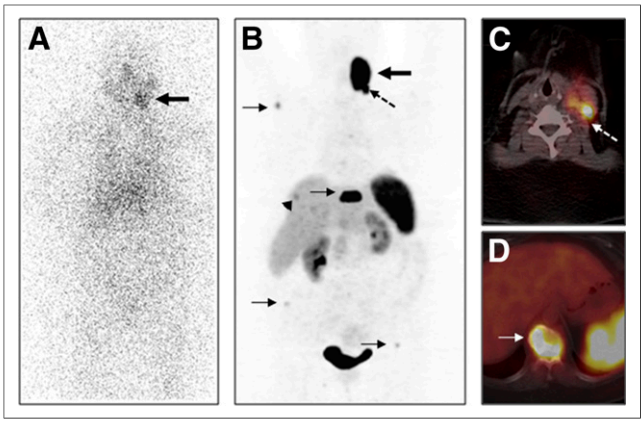

FIGURE 2. A 43-y-old woman with left CBT. Anterior ^{131}I-MIBG scintigraphy image (A) shows abnormal tracer uptake in left side of neck (bold arrow) corresponding to left CBT. No other focus of abnormal tracer uptake is noted. Maximum-intensity-projection ^{68}Ga-DOTANOC PET image (B) showed abnormal radiotracer uptake in left CBT (arrow) and multiple ^{68}Ga-DOTANOC–avid skeletal (arrow) and liver (arrowhead) metastases. Metastasis to left level II cervical node (B and C, broken arrow) was also noted. Collapse with intense tracer uptake is noted on 10th dorsal vertebra (D, arrow) suggestive of metastasis. Diagnosis of left CBT with nodal, liver, and skeletal metastases was made on ^{68}Ga-DOTANOC PET/CT and confirmed on follow-up.

is useful in this regard (*17*). SPECT or SPECT/CT with ^{123}I-/^{131}I-MIBG or ^{111}In-DTPA-pentetreotide SRS is generally used for this purpose. The latter is preferred because of the nonsecretory nature of HNPs. However, SPECT-based SRS has low resolution, resulting in higher chances of artifacts and attenuation, limiting the ability to detect small lesions. SPECT also does not provide a quantifiable estimate of tumor metabolism and has constraints such as long imaging time and delayed availability of results.

Although many paragangliomas predominantly express SSTR2, the receptor expression profile of metastatic lesion from these tumors is still not known. Hence, we used a broad-spectrum SSTR ligand (^{68}Ga-DOTANOC) having affinity for SSTR 2–5, as compared with ^{68}Ga-DOTATATE, which has affinity, although high, for SSTR 2 only (*9*). ^{68}Ga-DOTANOC PET/CT–based SSTR imaging has been shown to be useful for imaging HNPs in a few small series with mixed patient populations (*13–15*). Naswa et al. evaluated ^{68}Ga-DOTANOC PET/CT in a small series of 5 patients with CBTs (*15*). In that series, PET/CT demonstrated additional lesions in 3 of 5 patients (synchronous paragangliomas or metastasis), leading to a change in management. In another study, Naswa et al. (*13*) evaluated ^{68}Ga-DOTANOC PET/CT in patients with pheochromocytoma and paragangliomas, including 9 patients with HNPs. Although not separately mentioned, PET/CT showed a high accuracy and detected additional lesions in patients with HNPs. In the present study, ^{68}Ga-DOTANOC PET/CT showed excellent results for demonstrating HNPs. It showed 45 HNP lesions in these 26 patients. The size of the smallest HNP lesion seen on PET/CT was 0.8 cm. All HNPs seen on CT/MR imaging were seen on ^{68}Ga-DOTANOC PET/CT. As compared with contrast CT, ^{68}Ga-DOTANOC PET/CT demonstrated 7 additional head and neck lesions including 6 HNPs and 1 tumor thrombosis. On a lesion-wise comparison, ^{68}Ga-DOTANOC PET/CT was superior to conventional imaging (CT/MR imaging) ($P = 0.015$). Conventional imaging (CT/MR imaging) did not include imaging of the thorax–abdomen–pelvis. Early detection provides the opportunity to treat with a curative intent because these tumors are known to enlarge and cause significant local symptoms and debility. In addition, given its high specificity, ^{68}Ga-DOTANOC PET/CT is also able to confirm suspected head and neck lesions seen on CT/MR imaging as HNPs. However, other SSTR-expressing head and neck tumors such as carcinoid, medullary carcinoma thyroid, hemangiopericytoma, and melanoma can mimic HNPs on ^{68}Ga-DOTANOC PET/CT and should be kept in mind when interpreting such cases.

The major utility of ^{68}Ga-DOTANOC PET/CT lies in demonstration of synchronous paragangliomas at other sites (non-HNPs) and metastatic disease (*15*), which is critical because it can significantly affect patient management. In the present study, PET/CT demonstrated 10 non-HNPs. Of the 10 non-HNPs, 3 were mediastinal and 7 abdominal (including 2 pheochromocytoma). This is important because these tumors are usually surgically amenable. If left undetected and unattended, these non-HNPs can be the cause of catecholamine excess (because they are usually secretory) and debilitating symptoms. ^{68}Ga-DOTANOC PET/CT also detected 23 metastatic sites (the smallest lesion was 0.5 cm). Demonstration of metastatic lesions changed the therapeutic strategy from curative to palliative. The prevalence of metastatic HNPs in the present study population (6/26; 23% of patients) is higher than values reported in the literature (6%–19%) (*3*). These higher values

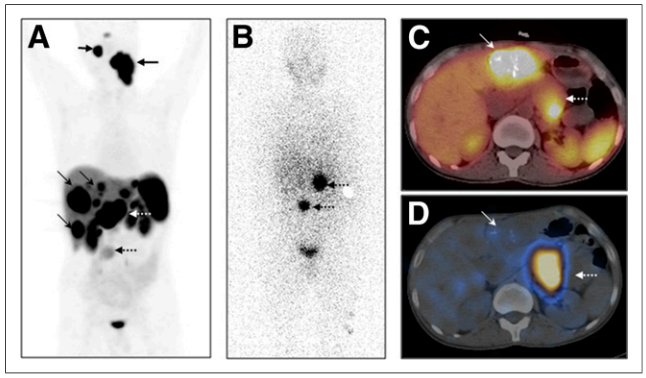

FIGURE 3. A 32-y-old man with left CBT and right glomus jugulare. Maximum-intensity-projection ^{68}Ga-DOTANOC PET image (A) shows tracer uptake in left CBT and right glomus jugulare (bold arrows), with multiple liver metastases (arrows) and 2 abdominal paragangliomas (A and C, broken arrows). Axial PET/CT image shows ^{68}Ga-DOTANOC–avid liver metastases (C, arrow). Anterior ^{131}I-MIBG scintigraphy image (B) shows 2 abdominal foci (broken arrows), which corresponded to retroperitoneal masses on SPECT/CT image (D, broken arrows), confirming paragangliomas. However, no ^{131}I-MIBG uptake was noted in CBT and glomus jugulare (B) or liver metastases (D, arrow).

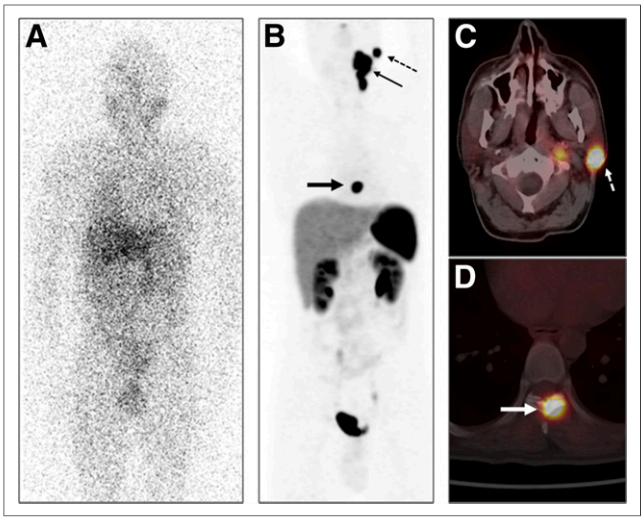

FIGURE 4. A 31-y-old man with left CBT. Anterior ^{131}I-MIBG scintigraphy image (A) was normal. Maximum-intensity-projection ^{68}Ga-DOTANOC PET image (B) shows abnormal radiotracer uptake in left CBT (arrow). Also noted were left parotid lymph node metastasis (B and C, broken arrow) and metastasis to left lamina of seventh dorsal vertebra (B and D, bold arrow). Primary tumor and nodal lesions were confirmed with fine-needle aspiration cytology. Patient was taken up for peptide receptor radionuclide therapy.

could possibly be due to a selection bias when sending patients with HNPs for staging with ^{68}Ga-DOTANOC PET/CT. Alternatively, the higher values could also be due to the improved detection of metastasis by ^{68}Ga-DOTANOC PET/CT. It must also be stressed that, in addition to the detection and localization of such tumors, ^{68}Ga-DOTANOC PET/CT provides the opportunity to demonstrate the in vivo expression of SSTRs, which can be exploited for treatment with peptide receptor radionuclide therapy.

On semiquantitative analysis, the SUVmax of the lesions varied widely (1.1–189.9). No overall correlation was seen between tumor size and SUVmax ($\rho = 0.027$; $P = 0.936$). A similar finding was reported by Naswa et al. (*13*). However, on subgroup analysis a significant positive correlation was seen between tumor size and SUVmax for HNPs ($\rho = 0.323$; $P = 0.030$). This could be due in part to partial-volume effect. The SUVmax ($P = 0.026$), but not the size ($P = 0.129$), of CBTs was significantly higher than that of jugulotympanic paragangliomas. The exact reason for this finding is not clear. Because the SSTR expression is increased in malignant paragangliomas (*12*), one can speculate that CBTs have more malignant potential than jugulotympanic paragangliomas. We also found that both size ($P = 0.029$) and SUVmax ($P = 0.047$) of non-HNPs were significantly less than those of HNPs. Because no correlation was seen between size and SUVmax of non-HNPS, it appears that the secretory and more benign nature of non-HNPs might have resulted in this difference.

The uptake of $^{123/131}$I-MIBG is dependent on the expression of vesicular monoamine transporters (1, 2) (*18*). The expression of vesicular monoamine transporter is high in benign pheochromocytoma but is reduced in malignant pheochromocytoma and paragangliomas, especially parasympathetic paragangliomas (HNPs). In the present study, ^{131}I-MIBG scintigraphy performed poorly. It demonstrated only 38.4% (30/78) of all lesions, only 35.5% (16/45) of HNPs, 60% (6/10) of non-HNPs, and 17.3% (4/23) of metastatic sites. Thus, use of ^{131}I-MIBG scintigraphy can lead to a gross underestimation of disease, especially distant disease, for which it is specifically used. On comparison, ^{131}I-MIBG scintigraphy was inferior to ^{68}Ga-DOTANOC PET/CT for HNPs (both CBTs and jugulotympanic paragangliomas) and metastases. One might argue that we have used ^{131}I-MIBG but not ^{123}I-MIBG, which allows a higher dose, gives a high photon flux, and provides better image quality and sensitivity (*19*). However, the sensitivity of ^{123}I-MIBG has also been reported to be low (18%–50%) for HNPs (*11,12*) and is comparable to the values for ^{131}I-MIBG seen in the present study. Hence, it is unlikely that use of ^{123}I-MIBG would have significantly altered the results. A combination of conventional imaging (CT/MR imaging) and ^{131}I-MIBG scintigraphy detected only 67.9% of lesions seen on PET/CT and no additional lesions. This combination was also inferior to ^{68}Ga-DOTANOC PET/CT ($P < 0.0001$).

Other PET tracers that can be used for imaging of HNPs include ^{18}F-FDG to assess glucose metabolism, ^{11}C-hydroxyephedrine and ^{18}F-fluorodopamine for determining catecholaminergic phenotype, and 6-^{18}F-fluoro-L-dopa (^{18}F-FDOPA) for assessing amine uptake and decarboxylation (*9*). Among these, ^{18}F-FDOPA appears to be most promising, with a reported sensitivity of 97% (*20,21*). It has been found to be superior to ^{111}In-DTPA-pentetreotide SRS for HNPs (*20,21*). This lower sensitivity of ^{111}In-DTPA-pentetreotide SRS probably is related to the limited resolution of SPECT. In addition, ^{18}F-FDOPA PET might miss extraadrenal retroperitoneal paraganglioma, which can potentially coexist with HNPs (*20*). Given the excellent results shown by both ^{18}F-FDOPA PET/CT and ^{68}Ga-DOTANOC PET/CT, a direct head-to-head comparison is warranted in HNPs. It is to be remembered that the difficult synthesis and limited yield of ^{18}F-FDOPA limits its wider availability, which is in contrast to the generator-based and easy synthesis of ^{68}Ga-DOTANOC. Although ^{18}F-FDG PET/CT has shown low sensitivity for primary paragangliomas, it shows high sensitivity for detection of metastasis from such tumors and is superior to ^{123}I-MIBG SPECT/CT, CT, and MR imaging for this purpose (*22*). In the present study population, ^{18}F-FDG PET/CT could have demonstrated additional metastatic lesions and might have played a role complementary to ^{68}Ga-DOTANOC PET/CT for metastatic HNPs. Germline mutations in genes encoding 1 of the subunits of the mitochondrial complex II succinate dehydrogenase (SDH) enzyme gene, a component of the tricarboxylic acid cycle, occur in a subset of HNP patients (*23*). The SDH status appears to be a critical parameter for determining the prognosis and for selecting the best functional imaging agent for paragangliomas (*24*). The impact of SDH status on ^{68}Ga-DOTANOC PET/CT imaging of paragangliomas,

including HNPs, is not yet known. Unfortunately, SDH status was not available for our patient population, and we were unable to evaluate its implications.

The present study is not without limitations. First, because of the rarity of HNPs the sample size was small, diminishing the power of the study. Second, this was a retrospective analysis with all its associated disadvantages. Third, ^{131}I-MIBG SPECT/CT was only available for 11 of 26 patients because at our center, similar to most others, the decision to perform SPECT/CT is guided by planar imaging. Fourth, in the absence of conventional imaging of the chest and abdomen or PET/CT with other tracers we could not definitely exclude non-HNPs when no such tumor was seen on ^{68}Ga-DOTANOC PET/CT. Because of this, we didn't calculate the lesion-wise diagnostic accuracy. Finally, the lack of knowledge regarding the SDH status, which is pivotal to understanding the results of functional imaging of HNPs, was a major limitation of the present study. Further larger prospective studies comparing ^{68}Ga-DOTANOC PET/CT with other functional tracers (especially ^{18}F-FDOPA PET/CT) and correlating imaging findings with SDH status are warranted.

CONCLUSION

The present study demonstrates the excellent results of ^{68}Ga-DOTANOC PET/CT for the baseline evaluation of HNPs. It is useful for detection and characterization of HNPs and to demonstrate synchronous paragangliomas at other sites and distant metastases. ^{68}Ga-DOTANOC PET/CT is superior to ^{131}I-MIBG scintigraphy and conventional imaging (CT/MR imaging) for this purpose. ^{68}Ga-DOTANOC PET/CT can become the modality of choice for functional imaging of HNPs if these results are confirmed in a larger population. Also, it can help in the selection of patients for peptide receptor radionuclide therapy if tumors are unresectable or metastatic.

DISCLOSURE

The costs of publication of this article were defrayed in part by the payment of page charges. Therefore, and solely to indicate this fact, this article is hereby marked "advertisement" in accordance with 18 USC section 1734. No potential conflict of interest relevant to this article was reported.

REFERENCES

1. Wasserman PG, Savargaonkar P. Paragangliomas: classification, pathology, and differential diagnosis. *Otolaryngol Clin North Am.* 2001;34:845–862.
2. Sykes JM, Ossoff RH. Paragangliomas of the head and neck. *Otolaryngol Clin North Am.* 1986;19:755–767.
3. Martin TP, Irving RM, Maher ER. The genetics of paragangliomas: a review. *Clin Otolaryngol.* 2007;32:7–11.
4. Hinerman RW, Amdur RJ, Morris CG, Kirwan J, Mendenhall WM. Definitive radiotherapy in the management of paragangliomas arising in the head and neck: a 35-year experience. *Head Neck.* 2008;30:1431–1438.
5. Boedeker CC, Erlic Z, Richard S, et al. Head and neck paragangliomas in von Hippel-Lindau disease and multiple endocrine neoplasia type 2. *J Clin Endocrinol Metab.* 2009;94:1938–1944.
6. van den Berg R. Imaging and management of head and neck paragangliomas. *Eur Radiol.* 2005;15:1310–1318.
7. Van den Berg R, Rodesch G, Lasjaunias P. Management of paragangliomas: clinical and angiographic aspects. *Interv Neuroradiol.* 2002;8:127–134.
8. van den Berg R, Verbist BM, Mertens BJA, van der Mey AGL, Van Buchem MA. Head and neck paragangliomas: improved tumor detection using contrast-enhanced 3D time—offlight MR angiography as compared with fat-suppressed MR imaging techniques. *AJNR.* 2004;25:863–870.
9. Taïeb D, Neumann H, Rubello D, Al-Nahhas A, Guillet B, Hindié E. Modern nuclear imaging for paragangliomas: beyond SPECT. *J Nucl Med.* 2012;53:264–274.
10. Kaltsas GA, Mukherjee JJ, Grossman AB. The value of radiolabelled MIBG and octreotide in the diagnosis and management of neuroendocrine tumours. *Ann Oncol.* 2001;12:S47–S50.
11. Koopmans KP, Jager PL, Kema IP, Kerstens MN, Albers F, Dullaart RP. ^{111}In-octreotide is superior to ^{123}I-metaiodobenzylguanidine for scintigraphic detection of head and neck paragangliomas. *J Nucl Med.* 2008;49:1232–1237.
12. Van der Harst E, De Herder WW, Bruining HA, et al. 123[I] Metaiodobenzylguanidine and 111[In] octreotide uptake in benign and malignant pheochromocytomas. *J Clin Endocrinol Metab.* 2001;86:685–693.
13. Naswa N, Sharma P, Nazar AH, et al. Prospective evaluation of ^{68}Ga-DOTANOC PET-CT in phaeochromocytoma and paraganglioma: preliminary results from a single centre study. *Eur Radiol.* 2012;22:710–719.
14. Naji M, Zhao C, Welsh SJ, et al. ^{68}Ga-DOTA-TATE PET vs. ^{123}I-MIBG in identifying malignant neural crest tumours. *Mol Imaging Biol.* 2011;13:769–775.
15. Naswa N, Kumar A, Sharma P, Bal C, Malhotra A, Kumar R. Imaging carotid body chemodectomas with ^{68}Ga-DOTA-NOC PET-CT. *Br J Radiol.* 2012;85:1140–1145.
16. Zhernosekov KP, Filosofov DV, Baum RP, et al. Processing of generator-produced ^{68}Ga for medical application. *J Nucl Med.* 2007;48:1741–1748.
17. Ayala-Ramirez M, Feng L, Johnson MM, et al. Clinical risk factors for malignancy and overall survival in patients with pheochromocytomas and sympathetic paragangliomas: primary tumor size and primary tumor location as prognostic indicators. *J Clin Endocrinol Metab.* 2011;96:717–725.
18. Kölby L, Bernhardt P, Johanson V, et al. Can quantification of VMAT and SSTR expression be helpful for planning radionuclide therapy of malignant pheochromocytomas? *Ann N Y Acad Sci.* 2006;1073:491–497.
19. Shapiro B, Gross MD. Radiochemistry, biochemistry, and kinetics of ^{131}I-metaiodobenzylguanidine (MIBG) and ^{123}I-MIBG: clinical implications of the use of ^{123}I-MIBG. *Med Pediatr Oncol.* 1987;15:170–177.
20. Charrier N, Deveze A, Fakhry N, et al. Comparison of ^{111}In pentetreotide-SPECT and ^{18}F FDOPA-PET in the localization of extra-adrenal paragangliomas: the case for a patient-tailored use of nuclear imaging modalities. *Clin Endocrinol (Oxf).* 2011;74:21–29.
21. King KS, Chen CC, Alexopoulos DK, et al. Functional imaging of SDHx-related head and neck paragangliomas: comparison of ^{18}F-fluorodihydroxyphenylalanine, ^{18}F-fluorodopamine, ^{18}F-fluoro-2-deoxy-D-glucose PET, ^{123}I-metaiodobenzylguanidine scintigraphy, and ^{111}In-pentetreotide scintigraphy. *J Clin Endocrinol Metab.* 2011;96:2779–2785.
22. Timmers HJ, Chen CC, Carrasquillo JA, et al. Staging and functional characterization of pheochromocytoma and paraganglioma by ^{18}F-fluorodeoxyglucose (^{18}F-FDG) positron emission tomography. *J Natl Cancer Inst.* 2012;104:700–708.
23. Timmers HJ, Gimenez-Roqueplo AP, Mannelli M, Pacak K. Clinical aspects of SDHx-related pheochromocytoma and paraganglioma. *Endocr Relat Cancer.* 2009;16:391–400.
24. Zelinka T, Timmers HJ, Kozupa A, et al. Role of positron emission tomography and bone scintigraphy in the evaluation of bone involvement in metastatic pheochromocytoma and paraganglioma: specific implications for succinate dehydrogenase enzyme subunit B gene mutations. *Endocr Relat Cancer.* 2008;15:311–323.

JNM The Journal of NUCLEAR MEDICINE

^{68}Ga-DOTANOC PET/CT for Baseline Evaluation of Patients with Head and Neck Paraganglioma

Punit Sharma, Alok Thakar, Sudhir Suman KC, Varun Singh Dhull, Harmandeep Singh, Niraj Naswa, Rama Mohan Reddy, Sellam Karunanithi, Rajeev Kumar, Rakesh Kumar, Arun Malhotra and Chandrasekhar Bal

J Nucl Med. 2013;54:841-847.
Published online: March 21, 2013.
Doi: 10.2967/jnumed.112.115485

The Journal of Nuclear Medicine is published monthly.
SNMMI | Society of Nuclear Medicine and Molecular Imaging
1850 Samuel Morse Drive, Reston, VA 20190.
(Print ISSN: 0161-5505, Online ISSN: 2159-662X)

SNMMI SOCIETY OF NUCLEAR MEDICINE AND MOLECULAR IMAGING